# ADVANCES IN PIXELVISION, INC. BACK-ILLUMINATED CCD IMAGING TECHNOLOGIES FOR LOW LIGHT LEVEL IMAGING APPLICATIONS

**July 1997**

**George M. Williams, James R. Janesick, Taner Dosluoglu, and Alice Reinheimer**

**PixelVision, Inc.**
**15250 NW Greenbrier Parkway**
**Beaverton, OR 97006**
**(503) 629-3210**
**www.pv-inc.com**

## ABSTRACT

With the goal of optimizing high resolution, low noise, back-illuminated CCD night vision imaging performance within the context of commercial manufacturability and cost effectiveness, PixelVision, Inc., in partnership with Scientific Imaging Technologies, Inc. (SITe) has undertaken, using its commercial Sandbox™ CCD processing service, a series of experimental design, performance optimization, and manufacturability efforts that has resulted in greater than 160 independent CCD designs. These low light level imagers have been demonstrated superior to conventional image intensified approaches for a broad range of night vision applications.

This paper describes a systems level approach by the authors to globally enhance all of the performance parameters of back-illuminated CCD technologies with the goal of manufacturing high yielding, cost effective imagers optimized for night vision applications.

We group the CCD performance parameters (which for low light level imaging must be simultaneously optimized) into four primary CCD operations:

1. Charge Generation (e.g. QE),
2. Charge Collection (e.g. MTF),
3. Charge Transfer (e.g. CTE), and
4. Charge Detection (e.g. Read Noise).

To demonstrate the process used to optimize these four CCD operations for night vision applications, this paper contains CCD Transfer Curve data for two PixelVision, Inc. Sandbox™ CCD devices. CCD Transfer Curves, a formal methodology of CCD test and optimization, is the only demonstrated method of characterizing all of the performance characteristics of a CCD in a single, context independent data set.

# Report Documentation Page

| Report Date | Report Type | Dates Covered (from... to) |
|---|---|---|
| 01JUL1997 | N/A | - |

| | |
|---|---|
| **Title and Subtitle**<br>Advances in Pixelvision, Inc. Back-Illuminated CCD Imaging Technologies for Low Light Level Imaging Applications | **Contract Number** |
| | **Grant Number** |
| | **Program Element Number** |
| **Author(s)**<br>Williams, George M.; Janesick, James R.; Dosluoglu, Taner; Reinheimer, Alice | **Project Number** |
| | **Task Number** |
| | **Work Unit Number** |
| **Performing Organization Name(s) and Address(es)**<br>PixelVision, Inc. 15250 NW Greenbrier Parkway Beaverton, OR 97006 | **Performing Organization Report Number** |
| **Sponsoring/Monitoring Agency Name(s) and Address(es)**<br>Director, CECOM RDEC Night Vision and Electronic Sensors Directorate, Security Team 10221 Burbeck Road Ft. Belvoir, VA 22060-5806 | **Sponsor/Monitor's Acronym(s)** |
| | **Sponsor/Monitor's Report Number(s)** |
| **Distribution/Availability Statement**<br>Approved for public release, distribution unlimited | |
| **Supplementary Notes**<br>See Also ADM201040 (1997 IRIS Proceedings on CD-ROM). | |
| **Abstract** | |
| **Subject Terms** | |
| **Report Classification**<br>unclassified | **Classification of this page**<br>unclassified |
| **Classification of Abstract**<br>unclassified | **Limitation of Abstract**<br>UU |
| **Number of Pages**<br>22 | |

## 1.0 INTRODUCTION

Back-illuminated CCDs with resolution greater than 4096 x 4096 elements, frame rates in excess of 10,000 frames per second, and noise lower than 3 electrons rms. have been independently demonstrated. Additionally, back-illuminated CCD cameras have been shown well suited for significant low light level imaging applications. However, the application of back-illuminated CCDs for night vision applications requires that all performance characteristics be optimized in a single manufacturable device. Unfortunately, there is a common tendency among manufacturers to optimize one CCD performance characteristic at the expense of others. Moreover, manufacturing methods employed for demonstrating *one* performance characteristic are often incompatible with the *global* performance parameters required of low light level imaging. To globally optimize CCD technologies for night vision imaging applications, the authors have developed a methodology of experimental design, process optimization, and absolute performance calibration. The goal of this effort is to develop superior back-illuminated CCD imagers, optimized for night vision applications, available in production level quantities, and procurable at cost effective prices.

### 1.1 PixelVision, Inc. Sandbox™ CCDs

To develop a comprehensive understanding of the fundamental principles governing CCD operation, PixelVision, Inc. has developed an on-going process of successive modeling, process optimization, and characterization. PixelVision, Inc. deploys this methodology in its Sandbox™ CCD foundry offering in which a number of CCDs are fabricated using a single mask set. The Sandbox™ provides the forum for development and evaluation of a number of experimental devices in a single fabrication lot without the expense of multiple mask sets and fabrication cycles. PixelVision, Inc. has used this same strategy to demonstrate the performance criteria of the low light level, back-illuminated CCD sensor.

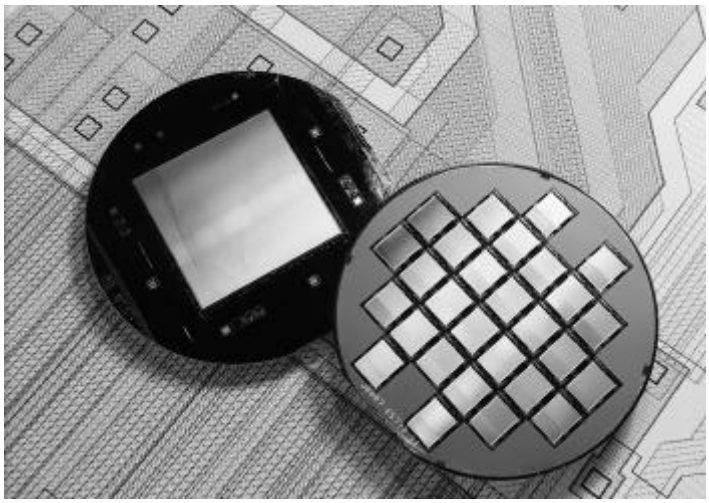

**Figure 1.1. Two Full Wafer CCD Designs. One with the Equivalent of 4096 x 4096, 12-micron square pixels (left); the other with over twenty-eight 652 x 976 element CCDs (right).**

Figure 1.1 illustrates two wafer designs that were fabricated on four-inch silicon wafers. The wafer on the left illustrates a 2" x 2" CCD design with the equivalent of 4096 x 4096, 12-micron square pixels. The design requires the full real estate of the four-inch silicon wafer. The right wafer shows a smaller design, a 652 x 976 element, frame transfer design that has 28 CCD die per wafer. As a single processing defect will render a device inoperable, it is easy to understand that the yield (and cost) of a

CCD increases as the area of the imager increases. Equally important are the increased complexity of the manufacturing processes, the photolithography techniques, and design parameters, all which change as devices increase in size and density.

The list of CCDs manufactured on PixelVision, Inc.'s *SandboxIII* and *SandboxIV* series of wafer designs is shown in Table 1.1. All of the forty CCD architectures were manufactured for back-illuminated CCD operation optimized for the visible and near infrared (VIS), ultra-violet (UV), or soft x-ray (NO). Additionally, front-illuminated CCDs (FR) were fabricated to offer a baseline for comparison – making a total of 160 different CCD designs available for characterization. Considering various operating modes such as progressive scan and interlaced readout modes, well over 300 very different SandboxIII and SandboxIV devices were available for characterization and integration with CCD camera electronics.

**Table 1.1. PixelVision, Inc. High Speed SandboxIII&IV CCD Designs**

| | CCD Model | Format | Number of Amplifiers | Amplifier Stages | Pixel Size (um) | QE Optimization | Readout Mode | Operating Mode | Architecture |
|---|---|---|---|---|---|---|---|---|---|
| | **PLUTO/III** | | | | | | | | |
| 1. | PV10KBVF2CH | 2048 x 1024 | 2 | 2 | 12 | UV,VIS,FR,NO | Progress./Interl. | NonMPP | Full Frame Transfer |
| 2. | PV10KBVF2MH | 2048 x 1024 | 2 | 2 | 12 | UV,VIS,FR,NO | Progress./Interl. | MPP | Full Frame Transfer |
| 3. | PV10KBVS4CH | 2048 x 1024 | 4 | 2 | 12 | UV,VIS,FR,NO | Progress./Interl. | NonMPP | Split Frame Transfer |
| 4. | PV10KBVS4MH | 2048 x 1024 | 4 | 2 | 12 | UV,VIS,FR,NO | Progress./Interl. | MPP | Split Frame Transfer |
| 5. | PV10KBVS4CH | 2048 x 1024 | 4 | 2 | 12 | UV,VIS,FR,NO | Progress./Interl. | NonMPP | Full Frame |
| 6. | PV10KBVS4CH | 2048 x 1024 | 4 | 2 | 12 | UV,VIS,FR,NO | Progress./Interl. | MPP | Full Frame |
| 7. | PV10KBVF2CH | 2048 x 1024 | 2 | 2 | 9 | UV,VIS,FR,NO | Progress./Interl. | NonMPP | Full Frame Transfer |
| 8. | PV10KBVF2MH | 2048 x 1024 | 2 | 2 | 9 | UV,VIS,FR,NO | Progress./Interl. | MPP | Full Frame Transfer |
| 9. | PV10KBVS4CH | 2048 x 1024 | 4 | 2 | 9 | UV,VIS,FR,NO | Progress./Interl. | NonMPP | Split Frame Transfer |
| 10. | PV10KBVS4MH | 2048 x 1024 | 4 | 2 | 9 | UV,VIS,FR,NO | Progress./Interl. | MPP | Split Frame Transfer |
| 11. | PV10KBVS4CH | 2048 x 1024 | 4 | 2 | 9 | UV,VIS,FR,NO | Progress./Interl. | NonMPP | Full Frame |
| 12. | PV10KBVS4CH | 2048 x 1024 | 4 | 2 | 9 | UV,VIS,FR,NO | Progress./Interl. | MPP | Full Frame |
| | **ADAPT** | | | | | | | | |
| 13. | ADAPTIII | 180 x 80 | 40 | 1 | 36 | UV,VIS,FR,NO | NA | NonMPP | Full Frame Transfer |
| 14. | ADAPTIII | 180 x 80 | 40 | 1 | 36 | UV,VIS,FR,NO | NA | MPP | Full Frame Transfer |
| | **FAST ONE** | | | | | | | | |
| 15. | FAST1 | 180 x 80 | 4 | 2 | 18 | UV,VIS,FR,NO | NA | NonMPP | Full Frame Transfer |
| 16. | FAST1 | 180 x 80 | 4 | 2 | 18 | UV,VIS,FR,NO | NA | MPP | Full Frame Transfer |
| | **NIGHTVIDEO** | | | | | | | | |
| 17. | PV652BVF2CH | 976 x 652 | 2 | 2 | 12 | UV,VIS,FR,NO | Progress./Interl. | NonMPP | Full Frame Transfer |
| 18. | PV652BVF2MH | 976 x 652 | 2 | 2 | 12 | UV,VIS,FR,NO | Progress./Interl. | MPP | Full Frame Transfer |
| 19. | PV652BVS4CH | 976 x 652 | 4 | 2 | 12 | UV,VIS,FR,NO | Progress./Interl. | NonMPP | Split Frame Transfer |
| 20. | PV652BVS4MH | 976 x 652 | 4 | 2 | 12 | UV,VIS,FR,NO | Progress./Interl. | MPP | Split Frame Transfer |
| 21. | PV652BVW4CH | 976 x 652 | 4 | 2 | 12 | UV,VIS,FR,NO | Progress./Interl. | NonMPP | Full Frame |
| 22. | PV652BVW4MH | 976 x 652 | 4 | 2 | 12 | UV,VIS,FR,NO | Progress./Interl. | MPP | Full Frame |
| | **PLUTO/IV** | | | | | | | | |
| 23. | PV10KBVF2CH | 2048 x 1024 | 2 | 2 | 12 | UV,VIS,FR,NO | Progress./Interl. | NonMPP | Full Frame Transfer |
| 24. | PV10KBVF2MH | 2048 x 1024 | 2 | 2 | 12 | UV,VIS,FR,NO | Progress./Interl. | MPP | Full Frame Transfer |
| 25. | PV10KBVS4CH | 2048 x 1024 | 4 | 2 | 12 | UV,VIS,FR,NO | Progress./Interl. | NonMPP | Split Frame Transfer |
| 26. | PV10KBVS4MH | 2048 x 1024 | 4 | 2 | 12 | UV,VIS,FR,NO | Progress./Interl. | MPP | Split Frame Transfer |
| 27. | PV10KBVS4CH | 2048 x 1024 | 4 | 2 | 12 | UV,VIS,FR,NO | Progress./Interl. | NonMPP | Full Frame |
| 28. | PV10KBVS4MH | 2048 x 1024 | 4 | 2 | 12 | UV,VIS,FR,NO | Progress./Interl. | MPP | Full Frame |
| | **KINO1** | | | | | | | | |
| 29. | KV10KBVS8CH | 2048 x 1024 | 4 | 1 | 12 | UV,VIS,FR,NO | Progress./Interl. | NonMPP | Full Frame Transfer |
| 30. | KV10KBVS8MH | 2048 x 1024 | 4 | 1 | 12 | UV,VIS,FR,NO | Progress./Interl. | MPP | Full Frame Transfer |
| 31. | KV10KBVS8CH | 2048 x 1024 | 8 | 1 | 12 | UV,VIS,FR,NO | Progress./Interl. | NonMPP | Split Frame Transfer |
| 32. | KV10KBVS8MH | 2048 x 1024 | 8 | 1 | 12 | UV,VIS,FR,NO | Progress./Interl. | MPP | Split Frame Transfer |
| 33. | KV10KBVS8CH | 2048 x 1024 | 8 | 1 | 12 | UV,VIS,FR,NO | Progress./Interl. | NonMPP | Full Frame |
| 34. | KV10KBVS8MH | 2048 x 1024 | 8 | 1 | 12 | UV,VIS,FR,NO | Progress./Interl. | MPP | Full Frame |
| | **KINO2** | | | | | | . | | |
| 35. | KV10CBVS8CH | 2048 x 1024 | 4 | 2 | 12 | UV,VIS,FR,NO | Progress./Interl. | NonMPP | Full Frame Transfer |
| 36. | KV10CBVS8MH | 2048 x 1024 | 4 | 2 | 12 | UV,VIS,FR,NO | Progress./Interl. | MPP | Full Frame Transfer |
| 37. | KV10CBVS8CH | 2048 x 1024 | 8 | 2 | 12 | UV,VIS,FR,NO | Progress./Interl. | NonMPP | Split Frame Transfer |
| 38. | KV10CBVS8MH | 2048 x 1024 | 8 | 2 | 12 | UV,VIS,FR,NO | Progress./Interl. | MPP | Split Frame Transfer |
| 39. | KV10CBVS8CH | 2048 x 1024 | 8 | 2 | 12 | UV,VIS,FR,NO | Progress./Interl. | NonMPP | Full Frame |
| 40. | KV10CBVS8MH | 2048 x 1024 | 8 | 2 | 12 | UV,VIS,FR,NO | Progress./Interl. | MPP | Full Frame |

Despite the variety of designs, the CCDs can be categorized into seven basic device families: 1) PlutoIII, 2) ADAPTIII, 3) FastOne, 4) NightVideo, 5) PlutoIV, 6) Kino1, and 7) Kino2. Each of the CCD families was designed to address and optimize one or more of the critical design characteristics required for video rate, low noise, and back-illuminated CCD operation.

In this paper, we detail the performance of two of the CCD families: 1) PlutoIII, and 2) ADAPTIII. The former was chosen because it represents the state of the art in low noise, video rate, low light level CCD sensor designs. Its features include multiple outputs (4 dual stage amplifiers), large format (2048 x 1024 element), low noise (less than 7 electrons rms.), and high frame rate (greater than 40 MHz bandwidth). The baseline Pluto architecture is shown in Table 2-1. The latter, the ADAPTIII, was chosen because, as it contains 40 closely spaced output amplifiers, it is an excellent test bed to easily perform orthogonal experiments and to establish manufacturing yields. As the physics and processing limits of CCD amplifiers is approaching theoretical limits, large format CCDs will increasingly rely on multiple output amplifiers for low-noise/low-light-level imaging.

## 1.2 CCD Operations, Performance Parameters, and CCD Transfer Curves

Low light level CCD performance parameters are grouped into four primary CCD operations: 1) Charge Generation (e.g. QE), 2) Charge Collection (e.g. MTF), 3) Charge Transfer (e.g. CTE), and 4) Charge Detection (e.g. Read Noise). Table 1.2 contains the four principle CCD operations required for low light level imaging, the performance parameters that comprise each operation, the CCD Transfer Curve(s) used to measure each parameter, and a list of influencing variables.

**Table 1.2. Four Basic CCD Operations and Associated Performance Parameters and CCD Transfer Curves Used to Measure Performance**

**1.2-1. Charge Generation Performance Parameters and CCD Transfer Curve Tests**

| Performance Parameter | Units | CCD Transfer Curve | Variables |
|---|---|---|---|
| **1. Quantum Efficiency (QE)** | Interacting Photons/ Incident Photons | QE Transfer | Wavelength, Temperature |
| **2. Quantum Efficiency Hysterisis (QEH)** | % modulation | Modulation Transfer | Clock Bias |

**1.2-2. Charge Collection Performance Parameters and CCD Transfer Curve Tests**

| Performance Parameter | Units | CCD Transfer Curve | Variables |
|---|---|---|---|
| **3. Pixel Non-Uniformity** | % rms. variation | Photon Transfer | Clock Bias |
| **4. Modulation Transfer Function (MTF)** | % modulation | Modulation Transfer | Clock Bias |

**1.2-3. Charge Transfer Performance Parameters and CCD Transfer Curve Tests**

| Performance Parameter | Units | CCD Transfer Curve | Variables |
|---|---|---|---|
| **5. Global CTE ($CTE_G$)** | Fraction of charge transferred | CTE Transfer | Charge Package Size, Temperature, Clock Rate and Bias, Clock Overlap |
| **6. Local CTE ($CTE_L$)** | Fraction of charge transferred | Bar Target Transfer | Charge Package Size, Temperature, Cock Rate and Bias, Clock Overlap |
| **7. Vertical Register Well Capacity** | Electrons | Photon Transfer<br>Full Well Transfer | Clock Bias, Clock Rate |
| **8. Horizontal Register Well Capacity** | Electrons | Photon Transfer<br>Full Well Transfer | Clock Bias, Clock Rate |

**1.2-4. Charge Detection Performance Parameters and CCD Transfer Curve Tests**

| Performance Parameter | Units | CCD Transfer Curve | Variables |
|---|---|---|---|
| **9. Node Sensitivity (Sv)** | V/e- | Photon Transfer | Temperature |
| **10. Amplifier Time Constant** | Sec | Video Transfer | Output Capacitance |
| **11. Linearity (γ)** | % | Linearity Transfer | On-chip Amp Bias, Signal Processing Chain |
| **12. Read Noise** | Electrons rms. | Photon Transfer<br>X-ray Transfer | Signal Processing/Analog Chain |
| **13. Dark Current Noise** | Electrons rms. | Dark Current Transfer | Temperature |
| **14. Spurious Charge** | Electrons rms. | Photon Transfer<br>X-ray Transfer | Clock Bias and Edges |
| **15. Dark Cosmetics** | Electrons/sec | Dark Transfer | Temperature |
| **16. Residual Image** | Electrons | Dark Transfer | Temperature, Signal, Integration and Read Time |

# 2.0 PLUTO ARCHITECTURE AND SUMMARY OF PERFORMANCE RESULTS

The following section summarizes the general architecture of the Pluto video rate, back-illuminated, low light level CCD as is outlined in Table 2-1.

The Pluto CCD is a video rate, low noise, 2048 x 1024 element, 9-micron or 12-micron pixel back-illuminated CCD. Using four high performance on-chip output amplifiers enhances the Pluto CCD's sensitivity and dynamic range. A high frame rate is maintained by using a Split Frame Transfer CCD design that has an opaque storage region on both the upper quarter and the lower quarter of the CCD array. Unlike interline transfer devices that often block more than 65% of incoming light, the Pluto CCD Split Frame Transfer architecture has 100 percent fill factor, thereby allowing every photon to strike the photo sensitive area of the CCD. This architecture optimizes the data transfer rate of the camera and minimizes image smear. As can be observed from the list of model variations in Table 1.1, the exact configuration of the CCD can easily be optimized for each application's requirements.

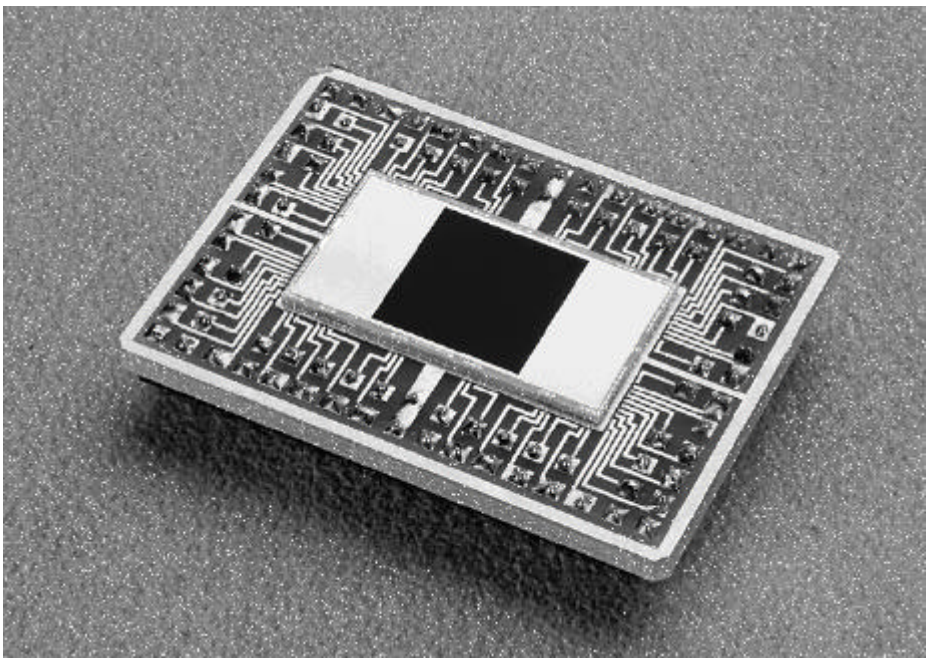

**Figure 2-1. Pluto 2048 x 1024 Element Split-Frame Transfer CCD**

**Table 2-1. Pluto CCD Family Architecture**

| | | |
|---|---|---|
| CCD Size | | 2048(V) x 1024(H) |
| Pixel Shape | | Square |
| Pixel Spacing | Pluto/9 | 9-microns |
| | Pluto/12 | 12-microns |
| Formats | Full Frame | One 2048(V) x 1024(H) imaging area |
| | Frame Transfer | One 1024(V) x 1024(H) imaging area<br>One 1024(V) x 1024(H) storage area |
| | Split Frame Transfer | One 1024(V) x 1024(H) imaging area<br>Two 512(V) x 1024(H) storage areas |
| Vertical Register Segments | | 4 quadrants independently bussed from both sides of the array |
| Horizontal Shift Registers | | Split |
| Summing Gates | | 4 |
| Output Transfer Gates | | 4 |
| Output Amplifiers | | 4 high speed, two stage MOSFETS |

A picture of a Split Frame Transfer version of the Pluto CCD is shown in Figure 2-1. When operating, the charge in the active, optically sensitive region of the CCD is clocked into the two storage regions, and while the signal from the next frame is being integrated, the charge in the storage region is sampled by correlated double sampling circuitry and is then digitized. Low noise, on-chip amplifiers are located on each corner of the CCD. Using four amplifiers decreases the noise equivalent bandwidth of the system and increases sensitivity.

Several PlutoIII CCD foundry lots were manufactured and the device performance was measured against the design goals. The high back-illuminated CCD quantum efficiency (greater than 85 percent), combined with multiple low noise amplifiers, results in a system that is ideally suited for low light level imaging applications. The back-illuminated, 2048 x 1024 element, four output amplifier, Pluto CCD is available with an anti-reflective coating that enhances the CCD's sensitivity in either the ultra-violet (UV), soft x-ray (NO) or visible (VIS) spectral regions. As can be seen in Table 2-2, which documents the performance measured for the design, the 12-micron Pluto CCD achieves less than 5 electrons rms. noise, full well exceeding 240,000 electrons, and linearity better than one percent.

**Table 2-2. SandboxIII PLUTOIII Performance**

| CHARACTERISTIC | | GOAL | ACHIEVED |
|---|---|---|---|
| **VERTICAL REGISTER** | | | |
| **Sensitivity (QE)** - *electrons per incident photon* | 4000A | >0.70 | >0.70 |
| | 6000A | >0.85 | >0.85 |
| | 8000A | >0.50 | >0.50 |
| **Charge Transfer Efficiency (CTE)** Fe-55 stimulus | | 0.99999 | 0.99999 |
| **Dark Current Noise** – 263 deg. K. (12-micron) | Partial Inversion (PI) | 10 | 10 |
| (electrons rms./sec) | MPP | 3 | 3 |
| **Vertical Full Well Capacity** | 9-micron/ PI | >50,000 electrons | >80,000 electrons |
| | 9-micron/ MPP | >25,500 electrons | >32,500 electrons |
| | 12-micron/ PI | >125,000 electrons | >240,000 electrons |
| | 12-micron/ MPP | >50,000 electrons | >85,000 electrons |
| **Vertical MTF** (at Nyquist) | 9-micron | 0.40 | TBD |
| | 12-micron | 0.30 | TBD |
| **Pixel Non-Uniformity** | | <3% | <2% |
| **Vertical Line Transfer** (at full well) | 9-micron | < 1 μsec | < 5 μsec |
| | 12-micron | < 1 μsec | < 5 μsec |

| | | | |
|---|---|---|---|
| **SERIAL REGISTER** | | | |
| **Charge Transfer Efficiency (CTE)** Fe-55 stimulus | | 0.99999 | 0.99999 |
| **Horizontal Full Well Capacity** | 9-micron | >150,000 electrons | >350,000 electrons |
| | 12-micron | >200,000 electrons | >500,000 electrons |
| **Horizontal Pixel Transfer** (at full well) | 9-micron | < 50 nsec. | < 50 nsec. |
| | 12-micron | < 50 nsec. | < 50 nsec. |
| **ON-CHIP AMPLIFIER** | | | |
| **Noise** (rms. at 300K) | | <3 e- rms. | < 5 e- rms. electrons |
| **Amplifier Sensitivity** | | >4 μV/e- | >3.5 μV/e- |
| **Video Dump Time Constant ($C_L$ = 5 pf.)** | | <25nsec | <25nsec |
| **Nonlinearity Over the Entire Dynamic Range** | | <1% | <1% |

## 3.0 CCD TRANSFER CURVES AND PLUTO CCD TEST DATA

This section presents photon transfer curve data used to calibrate performance parameters and test camera systems. Detailed performance characteristics and CCD transfer curves generated by the Pluto CCDs are presented. As introduced above in Table 1.2, performance parameters are grouped into four primary CCD operations:

**1. Charge Generation (e.g. QE),**

**2. Charge Collection (e.g. MTF),**

**3. Charge Transfer (e.g. CTE), and**

**4. Charge Detection (e.g. Read Noise).**

**3.1 Charge Generation:** Table 1.2-1 summarizes the performance characteristics that determine the charge generation capabilities of a CCD sensor – the ability to convert incident photons into signal photoelectrons – and the corresponding CCD Transfer Curves. Each Pluto CCD Charge Generation performance characteristic is discussed below.

**3.1.1 Charge Generation:** ***Quantum Efficiency (QE Transfer Curve):*** A back-illuminated CCD is capable of detecting photons over a huge wavelength spectrum (1.0A to 11,000A). Over most of this range, multiple electron-hole pairs are generated for each photon that interacts (multiple electron generation takes place for wavelengths shorter than 4000A). Figure 3.1 illustrates the quantum efficiency of SITe's CCD process for both front-illuminated operation and back-illuminated operation ).

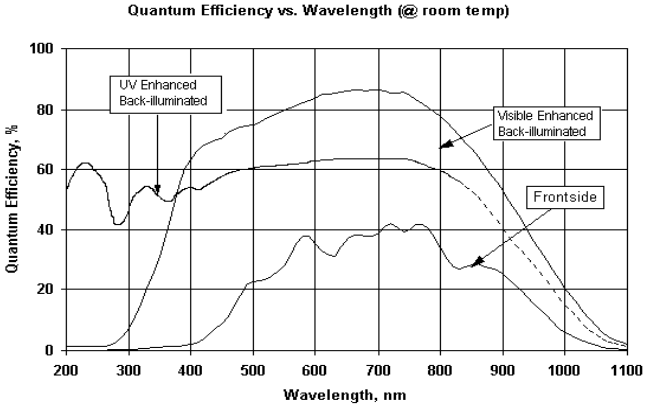


**Figure 3.1. Standard Scientific Imaging Technologies, Inc. (SITe) Quantum Efficiency Curve**

**3.1.2 Charge Generation:** ***Quantum Efficiency Hysterisis (QEH):*** Quantum Efficiency Hysterisis is an important parameter that measures the QE instability as a function of time, operating characteristics, and incident light. There are many physical factors that can contribute to this problem. Residual bulk image (RBI) is generated when signal charge interacts with the epitaxial/substrate interface. Charge that is trapped at that interface causes the QE to vary

from exposure to exposure. Unlike front-illuminated CCDS, back-illuminated CCDS have the substrate material removed and are not prone to RBI. However, due to the complex process required to accumulate the thinned surface of a back-illuminated CCD (resulting in nun-pinned" conditions), back-illuminated CCDS can exhibit unstable QE and Dark Current performance under high temperatures or under highlight conditions (especially in the UV where each photon has more energy).

QEH is calculated by measuring QE after a long period of stabilization under low light conditions, and then comparing that QE measurement with one obtained when the CCD is operating near full well. For near-infrared imaging (700nm - 1100nm), depending on a large number of operational conditions, stability better than one percent has been measured with the Sandbox™ Pluto CCD process.

3.2 **Charge Collection:** Table 1.2-2 summarizes the performance characteristics that determine the charge collection capabilities of a CCD sensor and the CCD Transfer Curve used to measure and optimize each performance parameter. In general, Charge Collection is the ability of the CCD to collect charge efficiently within the target pixels where the scene photons strike the CCD. Pixel non-uniformity and MTF are two key parameters that specify a CCD's charge collection efficiency (CCE).

3.2.1 **Charge Collection:** *Pixel Non-Uniformity (Photon Transfer Curve):* Some pixels in the array collect charge more efficiently than others – leading to pixel-to-pixel variation. These non-uniformities may be due to design and photolithography mask fabrication errors or processing contamination which might cause small pixel-to-pixel electric field potential variations.

The Photon Transfer Curve is used to quantify many CCD performance parameters, calibrate most of the other CCD Transfer and calibration curves, and optimize performance. It also serves as the main calibration curve for a camera system. For these reasons, it is one of the most important CCD Transfer Curves to generate, and is a convenient tool to quantify pixel-to-pixel variation. The Photon Transfer Curve (shown in Figure 3.2-1) simply plots noise as a function of signal for a population of CCD pixels. The mean and the variance of the CCD signal, from a uniform flat-field source of light, are encoded into a digital number (DN).

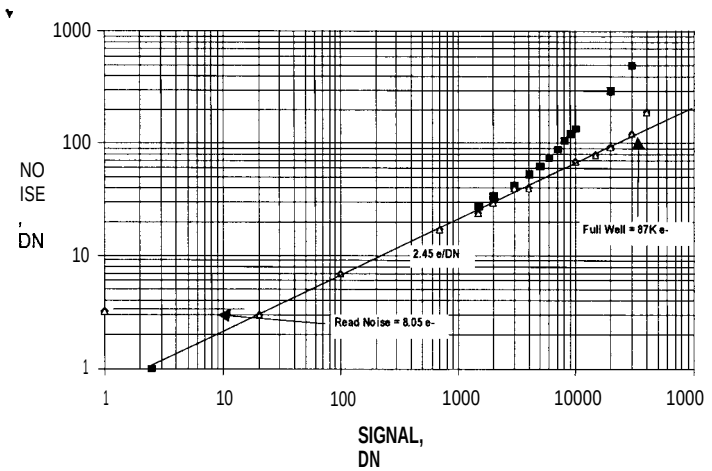


**Figure 3.2.1. Pluto 9-micron CCD transfer curve.**
**Portion of curve with slope ▫1 shows the pixel non-uniformity.**

Total noise is composed of three sources: 1) read noise, $\sigma_R$ (shown as a horizontal line at the bottom left hand side of the curve); 2) photon shot noise, $\sigma_{shot}$ (shown as the line with a slope of 1/2 – as predicted by the square root proportionality of shot noise phenomena); and 3) pixel non-uniformity noise, $\sigma_{PN}$ (a line with a slope of one). The CCD imager noise is the sum of these noise sources in quadrature:

$$\sigma_{s(DN)}^2 = \sigma_{R(DN)}^2 + \sigma_{shot(DN)}^2 + \sigma_{FP(DN)}^2$$

The magnitude of the pixel non-uniformity can be measured by determining where the signal's variance increases linearly with its mean (see Figure 3.2- 1). The point at which this line intercepts with the Shot Noise line (which increases with a slope of 1/2) shows the signal level at which pixel-to-pixel non-uniformity limits sensitivity.

Because pixel non-uniformities can be corrected using signal processing techniques, another method of obtaining the Photon Transfer Curve is to use two “difference” frames – one frame subtracted from the other – to remove fixed pattern noise from the analysis. This method is useful when measuring the CCD'S absolute linearity and full well characteristics. The Photon Transfer Curve performance measured using this technique represents the best performance achievable even with pixel correction.

Figure 3.2-2 shows a profile through a single line of the Pluto CCD under uniform exposure. As expected, some global offset non-uniformity is present due to dark current variation across the device (typically +/- 10 percent). A single pixel defect is also shown. The pixel does have response to light and can be compensated for with pixel correction electrons, albeit with degraded signal-to-noise performance. Figure 3.2-3 shows a histogram of pixel values for a uniform light source. As can be seen in the histogram, the curve is nearly gaussian suggesting that either readout noise or shot noise dominates performance. Fixed pattern noise and pixel defects are measured outside the region +/- 20f the distribution’s mean.

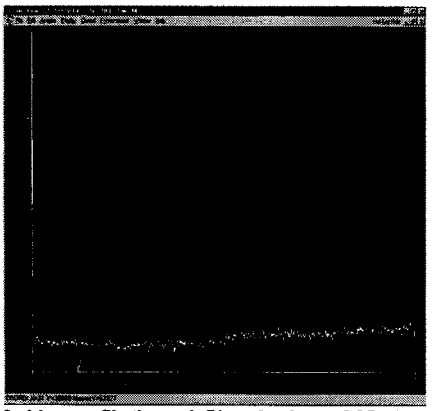

3.2-2. Line profile through Pluto 9-micron CCD showi uniformity

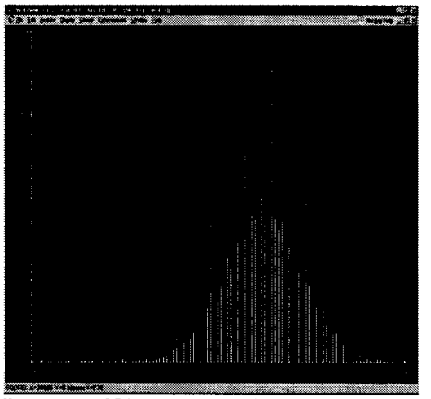

3.2-3. Histogram of Pluto 9-micron CCD. The Gaussian pe distribution, with few “outlayers”, illustrates good cosmetic quality and uniformity.

**3.2.2 Charge Collection:** *Modtdatwn Transfer Functwn @lTF/CTF Transfer Curve): The* Modulation Transfer Function (MTF) is a measure of the CCD'S ability to “spatially” reproduce the pattern of photons incident on the CCD. Ideally, the pixel-delineated region would collect every photon striking the CCD. However, there are many internal CCD mechanisms that can cause signal to wander from the target pixel into neighboring pixels. Disregarding the CCD'S sampling frequency (the inverse of a pixel-pair’s linear dimension), the primary mechanism that limits a CCDS MTF is the field free region beneath the CCD charge collecting well. If charge is collected outside of the CCD well and in the “field free" region, it will diffuse. The further from the “target” pixel’s potential well the photo-electron is created, the higher the probability that the signal will be collected in another pixel site.

The Contrast Transfer Function (CTF) is a sensor’s ability to image square waves, and it is in practice easier to measure than MTF. MTF and CTF are related through a geometric progression. Figure 3.2-4 shows a picture of a bar target imaged by the Pluto 9-micron CCDobtained with 5500A light. Figure 3.2-5 is a line profile through the bar target shown in Figure 3.2-4 from which CTF can be measured. The Pluto 9-micron CCD'S Nyquist limit is 55 line pairs per millimeter. The Nyquist limit of the Pluto 12-micron CCD is 31.6 line pairs per millimeter.

Due to absorption coefficients, 550nm light is collected by a front-illuminated CCD near the front surface and within the pixel’s charge collecting potential. For the back-illuminated CCD, the opposite is true, and the charge is collected near the back surface (away from the charge collecting region) and a portion of the charge

must diffuse before reaching a well potential. For “red” light, important for night vision applications, back-illuminated CCDS have superior CTF to the front-illuminated. This is because the red light travels further through the silicon and, for the back-illuminated CCD, will be collected close to the CCD'S front surface directly in the charge collection potential well. Alternatively, red light in a front-illuminated CCD may travel through the charge collecting region before generating a photoelectron. In this case, the charge must diffuse back to the potential well before being collected.

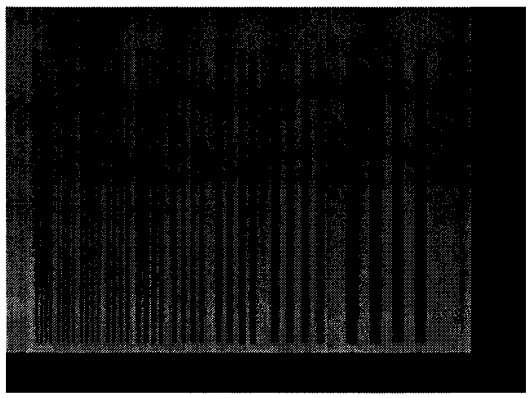

**Figure 3.2-4.**
**CTF Bar Target Image of Pluto 9-micron CCD**

Due to the fact that a thick epitaxial silicon is required to efficiently image the “red” and near-infrared (8000A to 11,000A) photons, there is a fundamental limit to the utility of small back-illuminated pixels for low light level imaging in the near infrared. The MTF degradation, especially in the shorter “blue” wavelengths, due to the diffusion of the photoelectrons in the thick epitaxy required for efficient collection NIR photons will dominate over the sampling frequency as determined by the pixel size. As a rule, a one-to-one correspondence between the thickness of the epitaxial material and the pixel size is recommended. Thus, since 12-micron epitaxal material is required for efficient NIR response, 12 microns is the smallest practical pixel geometry. For this reason, the Pluto 12-micron CCD has been shown to have superior MTF performance to the 9-micron pixel design.

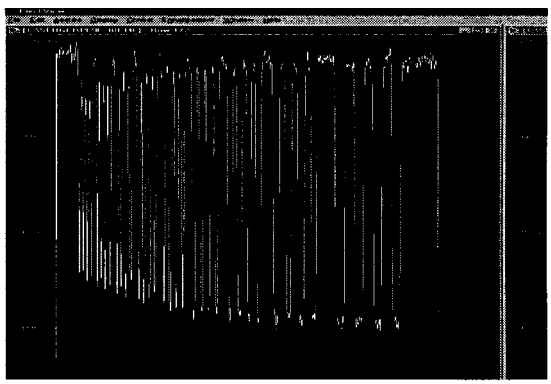

**Figure 3.2-5.**
**CTF Bar Target Line Profile of Pluto 9-micron CCD**

**3.3 Charge Transfer Efficiency Performance:** After charge is generated and collected by a pixel, it must be transferred to one or more of the amplifiers on the CCD. For very low light level imaging, there are a number of CCD characteristics that can interfere with the charge packet before it reaches the on-chip amplifier.

**3.3.1 Charge Transfer Efficiency:** *Global Charge Transfer Efficiency (X-ray Stacking Plot):* Charge transfer efficiency is measured as the ratio of the charge generated and collected in a CCD pixel’s well to the amount of charged measured at the output of the CCD. Deferred charge due to poor CTE can be spread over hundreds of pixels, degrading imagery and sensitivity, and making it difficult to account for all of the charge.

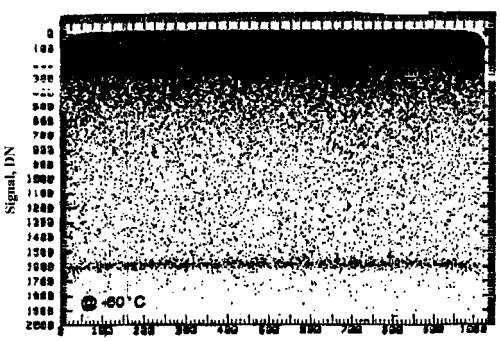


**CTE: Fe55 X-Ray Stacking Plot**
**Pluto 9-micron Horizontal Register**
**CTE T. Elliott – JPL**

**‘ Figure 3.3-1. X-Ray Stacking Plot**

A convenient method of measuring CTE in absolute terms is to use an x-ray source. Because the charge of an x-ray in silicon is known precisely, the amount of charge lost while transferring the charge generated by the x-ray photon can be calculated with certainty.

For example, a 5.9 keV, Fe55 produces 1620 electrons per event. Figure 3.3-2 shows a CTE curve for the Pluto 9-micron CCD.

As can be seen in the stacking plot, the strong response (the DN quivalent of 1620 electrons) represents a single pixel event line. The other strong lines represent "split" events shared by several pixels. A tilt in the line, representing lost charge, would indicate a CTE problem. As can be seen in the Figure, the CTE of the Pluto 9-micron CCD is nearly perfect and was measured to be 0.999995. This value indicates that an electron would be transferred 200,000 times before an electron would be "lost".

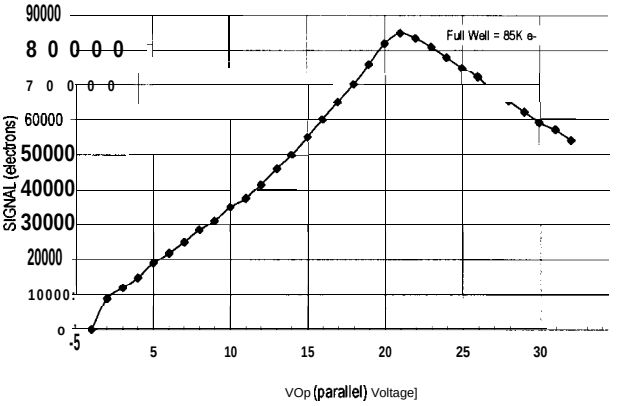


**Figure 3.3-2. Full Well Transfer Curve Showing Full Well Pluto 9-micron Back-illuminated (-60 degrees Celsius)**

3.3.2 **Charge Transfer Efficiency:** *Local Charge Transfer Efficiency:* CTE problems can occur that are associated with a single pixel. Traps extract a fixed amount of charge from charge packets as they are transferred through the image. Local CTE degradation can be caused by imperfections in the well structure caused by processing variations or incomplete photoresist removal. Also, crystal defects in the silicon can cause charge to be trapped while it is transferring through the dislocation site. X-ray, pocket pumping, Bar Target, and EPER are common methods of testing Local Charge Transfer Efficiency.

3.3.3 **Charge Transfer Efficiency:** *Parallel Full Well: (Full Well Transfer Curve):* For high-speed thinned CCDS, CTE problems can potentially develop. This is because the substrate, which normally acts as ground plane for front-illuminated CCDS, is lost in the thinning process. Hence, the ground impedance between the edge and center of the CCD significantly increases resulting in speed problems not encountered for non-thinned operation. The CTE effect is more pronounced for large array devices (>1024 x 1024 element CCDS working at 30 frames/see).

As shown in Figure 3.3-3, well capacity decreases as the clock frequency to the CCD is increased. The phenomena is related to "fringing fields". Fringing fields develop when there is a potential difference between phases. That is, potential on one gate will induce a fringing field under the edges of neighboring phases and, in turn, pull charge out of the phase. Without fringing fields, charge only moves from phase to phase by thermal diffusion aided by self-repulsion (both of which are relatively weak transfer processes). Fringing fields can extend several microns into neighboring phases when charge is absent, exhibiting maximum strength. However, as charge collects, the potential difference between phases is lowered resulting in smaller fringing fields. This is why it is much easier for a CCD to transfer small charge packets than large ones. At full well, fringing fields essentially disappear and charge transfer can only rely on diffusion and self-repulsion forces. Under full well conditions,

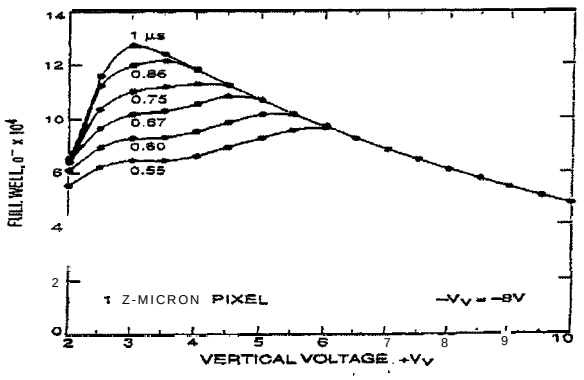


**Figure 3.3-3. High Speed Full Well Transfer Curve for a 12pm pixel. Note that the full well curve begins to change below 1 µsec. Clocking too fast causes the charge to bloom from the well.**

if the clocking rate is too fast, transfer will be incomplete and charge will bloom backwards. The family of curves shows that full well decreases with line transfer rate and with channel potential. As the transfer rate is increased, high channel potentials are required to maintain the same full well. This imposes constraints on the electronic clock drivers used.

3.4 **Charge Detection:** Table 1.2-4 summarizes the performance characteristics that determine the charge detection capabilities of a CCD sensor and the CCD Transfer Curve used to measure and optimize each parameter. Each will be discussed in detail below and the results of the SandboxIII Pluto CCD performance will be discussed.

3.4.1 **Charge Detection:** *Node Sensitivity (Photon Transfer Curve):* As described above, the Photon Transfer Curve simply plots noise as a function of signal for a population of pixels. The measured variance and mean signal levels are encoded into a digital number (DN) after being exposed to a flat-field source of light. The coordinates of the curve of Figure 3.4-1 are converted to absolute units of electrons by using the "system gain constant" (e-/DN). The conversion gain constant is calculated by assuming that the data is shot noise limited. By measuring the shot noise due to the number of electrons generated by interacting photons, statistics allows one to measure the number of electrons for each DN. This measurement requires that "difference frames", two identical flat-field image frames subtracted pixel by pixel, be generated at each exposure level. Fixed pattern noise ($\sigma_{FP}$) can thus be removed from the calculation. Figure 3.3-2 illustrates the full well transfer curve for the Pluto 9-micron CCD using the parallel gate phase voltages determined optimal for full well. Figure 3.4-1 is an expanded Photon Transfer Curve of the curve shown in 3.2-1, generated under high and low gain settings where the imaging area full well is reached. The full well value of 84,000 electrons, measured at the point where the signal's noise decreases as a function of increasing signal level (the noise over full well is correlated with the signal charge of adjacent pixels – thus decreasing shot noise), is in close agreement with the full well value calculated using the Parallel Voltage Transfer Curve (see Figure 3.3-2). Any difference in the two techniques is usually due to whether surface full well or bloomed full well conditions is reached first. These conditions are dependent on the clock bias potentials and the clock rates.

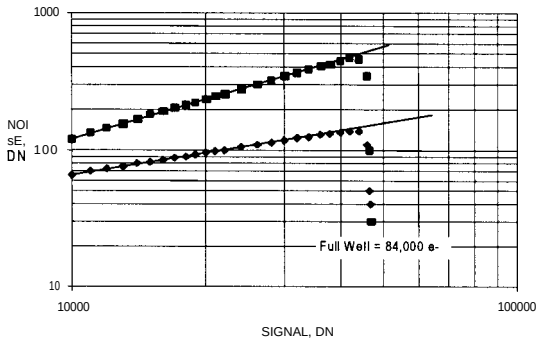


**Figure 3.4-1. Expanded Pluto/9 Photon Transfer Curve: High and Low Gain**

3.4.2 **Charge Detection:** *Linearity (Linearity Transfer Curve):* Linearity is the ability of the CCD to generate an output voltage in proportion to the charge contained in the pixel. Because linearity for the on-chip MOSFET amplifier is very good, ideally one would want the on-chip CCD amplifier to limit system linearity. Non-linearities less than 0.1 % are typical for on-chip, small pixel CCDS. Off-chip electronics are often 10/0 or greater.

Figure 3.4-2 shows a Linearity Transfer Curve that plots signal versus exposure time on log-log coordinates. The slope of the plot shows the constant gamma ($\gamma$), a parameter that quantifies the degree of proportionality between the charge transferred and the output voltage. Figure 3.4-3 shows the residual linearity error over the dynamic range of the CCD.

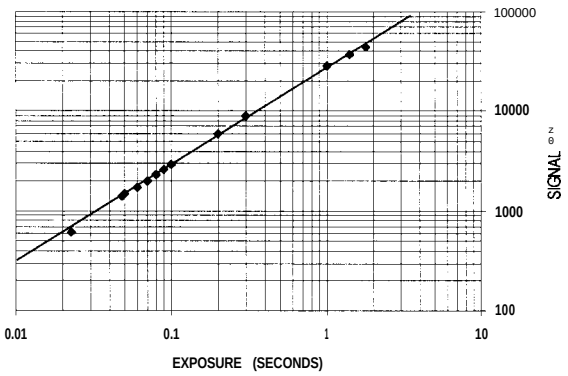


**Figure 3.4-2. Linearity Full Well Transfer Curve Pluto 9-micron back-illuminated CCD (T. Elliott.JPL)**

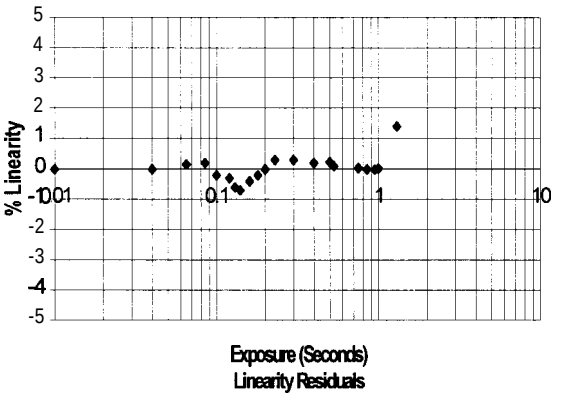


**Figure 3.4-3. Residual Linearity Measurement Pluto 9-micron back-illuminated CCD (1. Elliott-JPL)**

3.4.3 **Charge Detection:** *Dark Current Noise (Dark Current Transfer):* Single pixel spikes, dark current swirls that generate more than average dark current, luminescent shift registers, and amplifiers' poly-to-poly shorts that inject charge into the array are just a few of the dark current defects that can be measured. A Dark Current Transfer image identifies the location of the problem and quantifies the amount of dark current charge generated at a pixel site. The image is generated by integrating the charge for an extended period of time under dark conditions. Figure 3.4-4 shows the dark current generation rate as a function of CCD temperature for processes used to manufacture the back-illuminated Pluto.

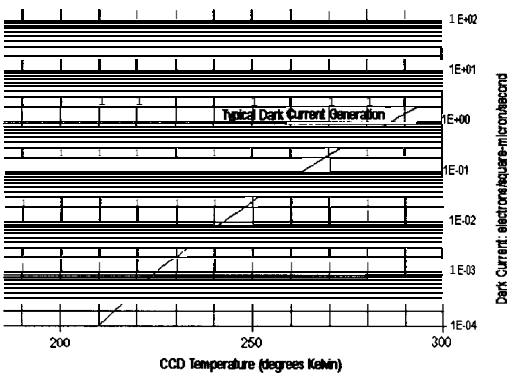


**Figure 3.4-4. Back-illuminated CCD Dark Current Transfer Curve (MPP Operation)**

3.4.4 **Charge Detection:** *Spurious Charge Noise (Photon Transfer Curve & X-ray Transfer):* When a CCD is driven into inversion, holes from the channel stops migrate and collect beneath the gate pinning the surface to substrate potential. Some of the holes can be trapped at the Si-Si02 interface. When the clock is switched to the non-inverted state, the trap electrons may accelerate out of the interface and into the silicon – generating electron-hole pairs. Spurious charge is generated linearly with the number of transfers that take place and can accumulate rapidly.

3.4.5 **Charge Detection:** *Read Noise (Photon Transfer Curve & X-ray Transfer):* The read noise can be seen in the Photon Transfer Curve of Figure 3.2-1. In the horizontal part of the curve, before the curve starts to rise proportionally with the square root of the exposure (shot noise), is the CCD'S readout noise. For the Pluto 9-micron CCD illustrated in the Figure, the noise was measured to be 8 electrons rms. Other Pluto CCDS demonstrated noise performance of 4.5 electrons rms, or better. Improvements in readout noise are likely as the Pluto CCD Transfer Curve optimization process (discussed below) evolves. Design and process improvements identified in this Sandbox™ effort,

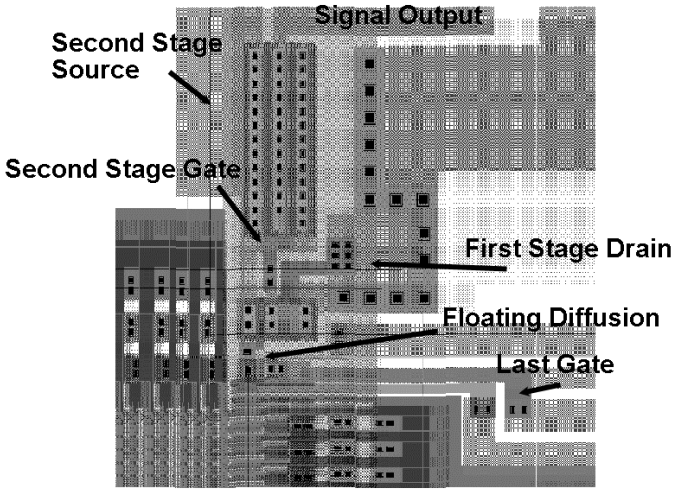


**Figure 3.4-5. Pluto Two-Stage Source Follower CCD Amplifier**

suggest that the noise can be improved to better than 2 electrons rms. without compromising manufacturability.

A detailed discussion of CCD amplifier noise optimization is given below as a precursor to the later discussions of the 40 output amplifier ADAPTIII Sandbox™ CCD design.

It is common practice to express CCD noise performance as the number of equivalent noise electrons. The square root of the product of the noise level (spectral density) and an equivalent noise bandwidth determine this figure of merit. A low value (high sensitivity) can be obtained in two ways: 1) a low noise spectral density, and 2) a small equivalent noise bandwidth. The equivalent noise bandwidth is determined by signal processing, and the CCD determines the noise electron density.

Due to fundamental semiconductor processing limitations, many manufacturers are approaching the theoretical limit of amplifier noise spectral density achievable with processes compatible for large area, low noise CCDs. Although there is slight room for improvement over the 4.5 electrons rms. measured for the Pluto CCD (the goal was <3 e- rms.), improvements in noise performance are achieved mostly by decreasing amplifier geometries. Gate widths less than one micron have resulted in amplifiers with approximately 1 electron rms. noise. However, as such tolerances are impractical for high resolution (large area) devices due to yield limitations and photolithography alignment limitations, the only method for achieving optimal low light level imaging performance is to use multiple output amplifiers.

There are three sources of noise in the floating diffusion type output amplifier of a CCD: 1) reset noise (channel resistance of the reset switch), 2) 1/f noise (flicker noise resulting from surface states related to the output transistor), and 3) white noise (thermal noise resulting from the channel resistance of the output transistor).

As discussed above, thermal noise cannot be eliminated, but can be considerably reduced by appropriate design and layout of the driver of the first source follower stage. The same is true for 1/f noise. Suitable design of a buried channel transistor can keep the 1/f noise component to an acceptable level. (At high operating speeds, 1/f noise is not a major contributor to a CCD's noise performance.) On the other hand, it is very difficult to get rid of reset noise at the CCD level. Techniques such as correlated double sampling (CDS) or delay-line processing in the analog signal chain are used to drastically lower the influence of the reset noise. At high data rates, such circuitry becomes increasingly complex.

A pixel data rate dependent optimum amplifier geometry does exist. As the pixel rate increases, the processing time given to each pixel becomes shorter (we assume in this discussion that correlated double sampling is employed). Reducing the sample time lowers 1/f noise generated by the output amplifier, because low-frequency noise components become correlated. Reducing 1/f noise through signal processing allows one to reduce the size of the on-chip amplifier. This in turn increases the

sensor's sensitivity (V/e-) because of reduced gate capacitance associated with the first stage MOSFET amplifier. Noise (i.e., electrons rms.) is reduced proportionally. However, as the amplifier becomes smaller, its transconductance (V/A) decreases resulting in a greater white noise floor. This results in higher noise and sets the limit of how small the device can be. Thus, for a given sample time (a given data rate), the point where white and 1/f noise increases more than the sensitivity increases defines the optimum amplifier size. The white noise has a weak dependence on the channel width of the source follower MOS transistor near its optimum value. It depends more strongly on bias current and channel length. With a simple MOS transistor model, it is possible to calculate the optimum value of the channel width, which has been proven by several sources, including PixelVision, Inc., to be in good agreement with measured results.

The discussion above shows that minimum noise and maximum low light sensitivity is achieved when sensitivity is high and white noise is low. Down to a certain amplifier size, the decrease in the first stage's capacitance increases sensitivity at a faster rate than white noise, thus the signal to noise ratio is improved. Ultra-small amplifiers are advantageous for fast-scan applications where 1/f noise is not important. This is because $T_s$ is small and 1/f noise remains correlated. Under such conditions, white noise is the only noise source that needs to be considered. However, there is still a limit to how small the amplifier can be made. As the gate capacitance decreases with size, parasitic capacitance becomes more important. Hence, parasitic capacitance and white noise will eventually limit size. The equations presented here bracket the problem and demonstrate what is involved in the optimization process.

## 4.0 MULTIPLE OUTPUT CCD OPTIMIZATION

As discussed above, it is common practice to express CCD noise as the square root of the product of the noise level (spectral density) and an equivalent noise bandwidth. By definition, a low value (better sensitivity) can be obtained in two ways: 1) a low noise spectral density, and 2) a small equivalent noise bandwidth.

For the reasons described in the section above, we are rapidly approaching the limits to decreasing the noise spectral density of on-chip CCD amplifiers using smaller amplifier geometries. For this reason, PixelVision, Inc. has focussed on producing CCD designs with multiple output amplifiers to reduce the *noise equivalent bandwidth*. The ever-increasing density of commercially available signal processing electronics, which makes the integration of CCDs with a large number of output amplifiers realizable, supports this approach.

Our testbed for optimizing multiple output CCDs is our ADAPTIII CCD – a very high frame rate (10,000 frames per second), low noise (less than 3 electrons rms.), back illuminated CCD designed for adaptive optics and wavefront sensing applications. The imaging area consists of nominally 80 x 80, thirty-six μm square pixels. It utilizes full frame transfer architecture with an additional nominal 80 rows in the storage region. To achieve low noise at high speeds, 40 on-chip amplifiers are used. The signal charge from every two columns is mixed together into one output amplifier. Thus, the 40 output amplifiers operate in parallel to provide high frame rates at very low noise operation. Each amplifier senses first the charge from one column, then the charge from the other.

The specifications of the PixelVision, Inc. ADAPTIII CCD are shown below:

**Table 4-1, ADAPTIII Architecture and Performance**

| | |
|---|---|
| 1. Pixel Format | 320(v) X 80(h) |
| 2. Pixel Shape | 18 μm (v) x 36 μm (h) |
| 3. Effective Pixel Size (binned horizontally) | 36 μm (v) x 36 μm (h) |
| 4. Architecture | Full array or split-frame transfer |
| 5. Binned Pixel Shape: | Square |
| 6. Pixel Spacing | 36-microns |
| 7. Output, low noise, floating diffusion, LDD, buried-channel, single-stage, MOSFET amplifiers | 40- one for every two columns |
| 8. Frame Rate | Greater than 10,000 |
| 9. Readout Noise | Less than 3 e- rms. at 1,200 fps |

The purpose of this set of measurements was to (1) verify functionality of the back-illuminated design, (2) optimize operating voltages, and (3) measure performance parameters. Successful demonstration of all 40 amplifiers, all in close proximity to one another, and operating with a common set of bias lines and signal chain electronics, significantly reduces risk of future, large area, multiple output CCD designs.

In addition to the 40 output amplifiers, the ADAPTIII CCD also has a conventional serial register adjacent to the imaging area. This register was used to verify the CCD cosmetic quality. The CCD was found to have no blemishes greater or less than +/- 20°/0 of the average response at an illumination equivalent to half of the pixel full well value.

To find the optimum ADAPTIII amplifier operating voltages, a representative amplifier of the 40 (output 11) was characterized. The voltage optimization technique used is described in Section 5.0 and is shown in Figures 5.2-1 and 5.2-2. The amplifier threshold was measured to be 14.5 volts. Charge Transfer Efficiency (CTE) was verified using an Fe55 x-ray source. The measurement was also used for gain calibration.

Figure 4-1 shows readout noise plotted in electrons (rms). for each of the forty amplifiers. As can be seen from the plot, all forty of the ADAPTIII CCD amplifiers operate with less than 4 electrons rms. noise. The conversion gain of the amplifiers was found be approximately 2.0 ~V/electron.

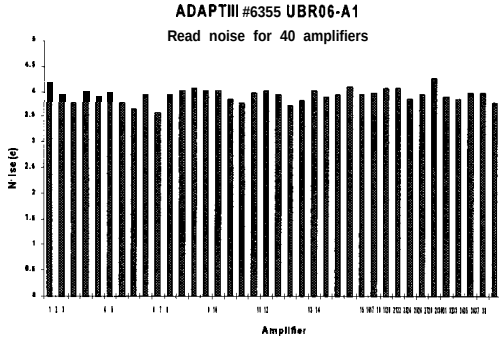


**Figure 4-1. Output Amplifier Noise for Forty ADAPTIII Amplifiers**

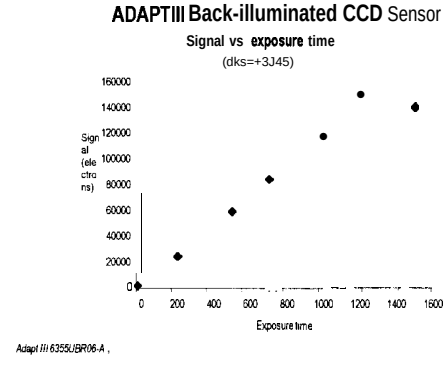


**Figure 4-2. Full Well and Linearity Measurement**

Figure 4-2 shows a plot of signal versus exposure time. To make these measurements, increasing the exposure time under constant illumination flux density increased the input illumination. As can be seen from the plot, signal increases linearly up to at least 140,000 electrons, at which point overflow of the adjacent pixels causes the shot noise to decrease as a function of increased light exposure.

## 5.0 OPTIMIZING SANDBOX™ CCD CLOCK WAVEFORM AND BIASES

Not only are the CCD Transfer Curves useful for characterization, they also serve as an invaluable tool for the optimization of the CCD's clock waveform and biases. This section contains a description of the CCD Transfer Curve method of CCD optimization and provides CCD Transfer Curve data used to determine the ideal operating parameters of the Pluto CCD. All CCD performance characteristics depend on camera clock drive, bias, and off-ship signal processing parameters. Rather than use a trial and error approach to CCD optimization, Jim Janesick, Chief Scientific Officer for PixelVision, Inc., developed the CCD Transfer Curve method for CCD optimization. The approach is detailed below and is described in more detail in ***Janesick, James R., "CCD Transfer Curve Method - Standard for Absolute Performance of CCDs and Digital CCD Camera Systems", SPIE, San Jose, February 1997.***

A diagram of the output register of the Pluto CCD is shown in Figure 5-1 and illustrates the setup clock waveform and DC potentials for the last three pixels of the serial shift register ($V_s$), before it is collected in the Summing Well ($V_{sw}$), transferred to the Last Gate ($V_{otg}$), and then sampled by the output MOSFET, when the charge is dumped to the output node using the amplifier with a Voltage Reference ($V_{ref}$), Reset Gate ($V_{rg}$), and output drain ($V_{dd}$). This picture provides a visual aide that assists in the understanding of the methodology used to optimize PixelVision, Inc.'s CCDs.

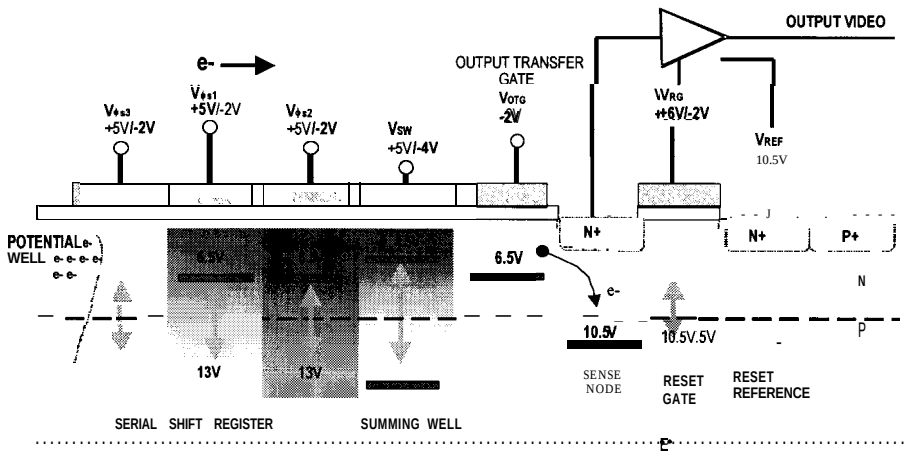


**Figure 5-1. CCD Output Showing Example Setup and DC Potentials**

**5.1 Output Transfer Gate (OTG) Transfer Curve:** The last gate (the output transfer gate, OTG) is the first critical voltage that is set when optimizing and characterizing the Pluto CCD. It is the voltage that is used to set all of the other CCD clock and bias voltages. The threshold potential ($V_{eff}$), is a CCD constant that is used to determine the maximum channel potential ($V_{max}$), beneath a gate electrode when it biased to $V_g$. The channel potential well beneath a gate electrode extends 3.5 to 4.5 microns into the silicon. Maximum potential ($V_{max}$), is at its maximum near the surface where signal electrons are first collected. The collecting phase is the phase which is biased high (say 3 volts) and collects photoelectrons. The barrier phase is biased low (say to –8 volts) and confines

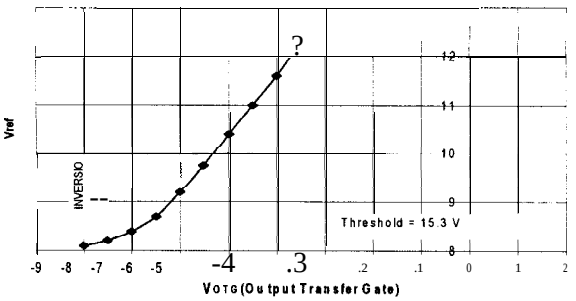


**Figure 5.1-1. Output Transfer Gate Transfer Curve Pluto/12 # PV12A (J. Janesick-PV)**

charge to the collecting phase. $V_{eff}$, the maximum channel potential, is found from the OTG Transfer Curve.

When the potential of the Output Transfer Gate (OTG) is elevated, the channel potential will increase linearly until it becomes equal to the potential of the sense node that physically overlaps the region. Due to the sampling process, the channel potential is reset to $V_{ref}$ when the Reset Gate is switched on. When the maximum channel potential ($V_{max}$) is greater than the reset voltage (V,.f), then the electrons from the sense node will flow under the Output Transfer Gate because its potential is lower. When $V_{max} > V_{ref}$, the electrons flowing under the Output Transfer Gate will result in "charge injection" into the CCD. The breakpoint is called "clock punch-through" because of the sudden clock feed-through signal that is observed at the output of the CCD.

Before $V_{otg}$ can be set to a specific voltage potential, one other important breakpoint for the CCD is required. When a phase is driven sufficiently negative, the surface potential at the Si-$Si0_2$ interface will eventually reach the same potential as $V_{sub}$, which is normally set to O volts. When this occurs, holes from the substrate and surrounding p+ material populate the interface and "pin" the surface potential to the substrate potential. This state is called "inversion" ($V_{inv}$), because majority of carriers for n-material, which are used to dope the material, are electrons. Under these conditions, the potential at the surface and throughout the silicon is fixed and is independent of the gate voltage applied.

Knowing $V_{eff}$, $V_{inv}$, and VOW, the "operating window" of the bias points that accommodated device and process variation, puts one in an excellent position to select the other CCD operating parameters one-by-one. The Output Transfer Gate is set to an operating range that centered in the operating window, VOW, above the onset of inversion.

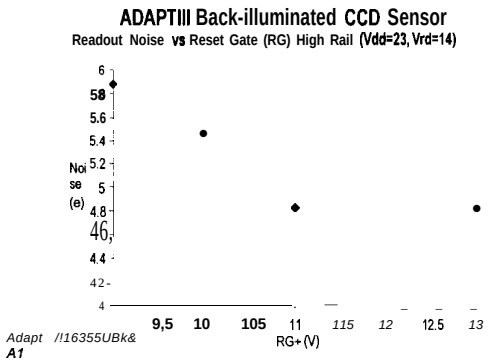


**Figure 5.2-1. Amplifier Noise as a Function of Amplifier Reset Gate Voltage**

5.2 **Amplifier Voltage Reference / OTG Transfer Curve & $V_{dd}/V_{rd}$ Transfer:**

For the ADAPTIII CCD, it can be seen that if the Output Transfer is set to -4 volts, then the optimal amplifier noise can be achieved with the voltage settings of $V_{dd} = 24$ volts, and $V_{rd} = 13.5$ volts.

Amplifier noise was measured with the CCD cooled to 250K and the charge clocked away from the output amplifier. After optimizing the Output Transfer Gate voltage, in a method similar to that discussed above, the noise of the amplifier was measured as a function of the Reset Gate of the output amplifier. As is shown in Figure 5.2-1, above a $V_{rd}$ voltage setting of 11 volts the amplifier completely resets and noise decreases. Tests demonstrated that the "high" rail of the Reset Gate is optimally operated above 13

volts to provide a complete reset. Choice of the V,d setting must take into account the signal swing as well as processing variation. For this reason, a voltage setting of 13.5 volts was used – assuming a 2 volt signal swing and an operating process window of 13.5 volts. Next, the optimal $V_{dd}$ setting was chosen by plotting noise versus $V_{dd}$ voltage settings. Although the gain of the output FET increased with increasing $V_{dd}$ to $V_{rd}$ voltage (See Figure 5.2-2), the noise floor starts to increase when the charge carriers reach the surface close to the gate Si-$Si0_2$ interface. This point is represented by the knee of the curves in Figure 5.2-3. Shown in Figure 5.2-3 are the $V_{dd}/V_{rd}$ Transfer Curves for three gate-to-drain ($V_{rd}$) settings. A $V_{rd}$ setting of 13.5 volts exhibits optimal noise performance. The amplifier voltage reference is set to a potential just above (taking into account VOW) the onset of clock punch-through. In addition, extra latitude is given $V_{ref}$ because the potential in the sense node, due to signal charge, moves in the direction of punch-through when charge is in it. As signal swings can often exceed **2** volts, sufficient margin must be given when setting the operating voltages to accommodate the largest signal swings required of the application as well as processing variations.

These transfer curves are generated for each manufactured CCD lot to verify that the operating conditions of the electronics are optimized for the operating window offered by the CCD process.

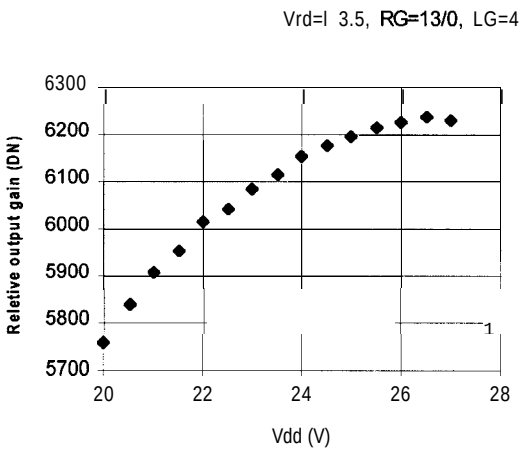


**Figure 5.2-2. Gain as a Function of Vdd (Vrd=13.5V)**

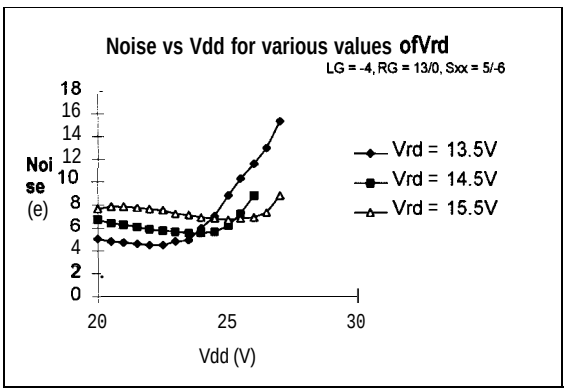


**Figure 5.2-3. Noise as a Function of Vdd for Various Vrds**

## 6.0 OTHER SANDBOX™ CCD DESIGNS

**6.1 Kino 2048 x 1024, Eight Output CCD Design:** On the center/right of the SandboxIV wafer is an 8-output design that uses a similar cell structure to the Pluto CCD. This design has been named ***Kino.*** The primary functional difference between Pluto and Kino is the number of amplifiers. Kino has 8 output amplifiers and Pluto has 4 output amplifiers. As the noise of a CCD is proportional to the square root of the bandwidth, the CCD demonstrates the 40 percent sensitivity improvement that is a result of moving to twice as many amplifiers. Issues such as cross talk, electronics complexity, and amplifier yield will be addressed in the characterization of the Kino design. Many of these issues were addressed with the SandboxIII ADAPTIII CCD design, which, as described above, has forty output amplifiers.

The Kino was designed with two basic configurations. The top two devices on the center of the wafer are designed with amplifiers that use a two-stage output structure. To demonstrate the tradeoffs between one- and two-stage amplifiers, a one-stage amplifier design of the Kino CCD was

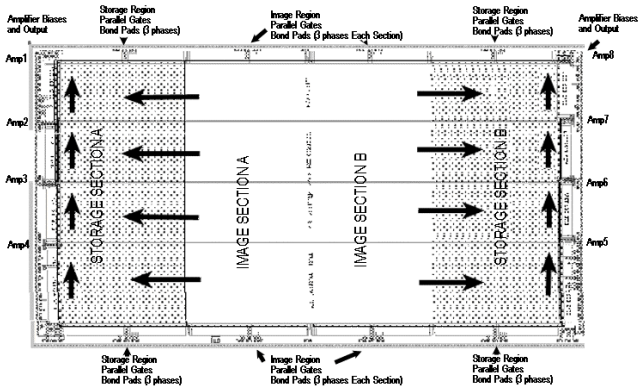


**Figure 6.1. Kino, 8-output, 2048 x 1024 SandboxIV CCD Design**

also included in this Sandbox™ wafer. One-stage amplifier designs are usually superior at data rates below 500Kpix/sec. As one of the goals of this program was to demonstrate the superior performance of multiple output amplifiers with low noise, the possibility of large arrays with multiple output amplifiers may result in one-stage amplifier structures. This program will assess the performance expectations of such a design. The Kino 8 output CCD design is shown in Figure 6.1.

**6.2 NightVideo™, 976 x 488 Element, Four Output CCD Design:** The third core design located on the far right of the SandboxIV wafer is a 976 x 488 element NightVideo™ CCD design that can be manufactured with Split Frame Transfer, Full Frame Transfer, or Full Frame architectures. The CCD uses the two-stage amplifier found on the Pluto and the two-stage Kino design and is available with both MPP and non/MPP operation. The CCD can be operated in 30Hz progressive or 60Hz interlaced mode.

## 7.0 APPLICATION OF BACK-ILLUMINATED CCD TECHNOLOGY

As indicated in the absolute performance characterization detailed above, low noise, back-illuminated, low light level CCD (BCCD) cameras offer superior low light level performance to image intensified approaches. With wideband spectral response, a better spectral match to the night sky than GenIII image tubes, over 14-bits of dynamic range, high MTF, and anti-blooming protection, these images offer better sensitivity than image intensified approaches. This results in greater transmission of information to the user.

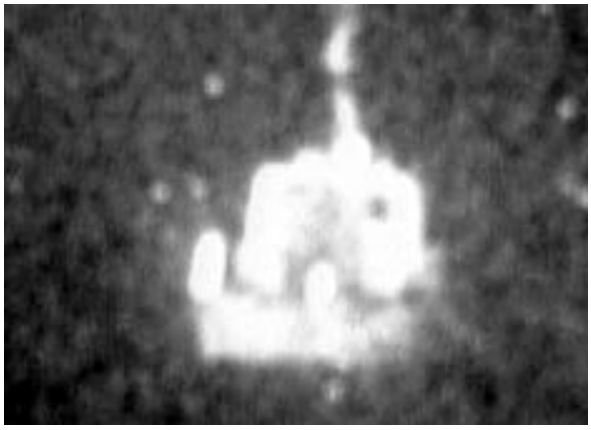

**Figure 7-1. Actively Illuminated image of a boat at 520 meters – acquired with a GenIII image intensified CCD camera**

**Figure 7-2. Actively Illuminated image of a boat at 520 meters – acquired with a PixelVision, Inc. back-illuminated CCD camera**

The back-illuminated CCD uses a dramatically different approach to low light level imaging. Rather than relying on gain, which degrades the signal to noise of the imager, the BCCD increases the

responsivity with respect to the night sky radiance, fill-factor, contrast, and MTF of the imager to improve the signal to noise of the resulting target image – especially at high spatial frequencies. This allows for superior resolution and contrast low light level imaging at low light levels. With the combination of high MTF and high sensitivity, the BCCD video sensor provides imaging of scenes that cannot be achieved with conventional CCDs and for which ICCDs suffer from low contrast and resolution. Thus, the BCCD is a superior sensor to ICCD approaches.

Figures 7.1 and 7.2 show a side-by-side comparison of a back-illuminated CCD low light level imager and a GenIII image intensified imager (images courtesy of FLIR Systems [Portland, OR]).

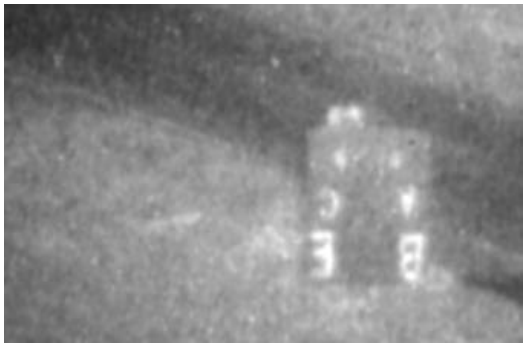

**Figure 7-3. Actively Illuminated image of bar targets at 400 meters – acquired with a GenIII image intensified CCD camera**

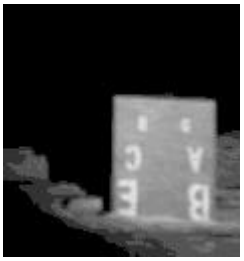

**Figure 7-4. Actively Illuminated image of a boat at 400 meters – acquired with a PixelVision Inc. back-illuminated CCD camera**

The boat is at a range of approximately 520 meters. As can be seen in the images, the running lights and the reflections off surfaces of the boat cause the image intensified imager to bloom – making it useless for identification purposes. The low light level back-illuminated CCD imager clearly identifies the resolution target on the back of the boat, as well as identification markings. In tests by FLIR Systems and USAF Phillips Laboratories, range to recognize 6-inch letters was shown to be just under 600 meters, and 1100 meters for 12-inch letters.

Figures 7.3 and 7.4 show a similar test of bar targets clearly illustrating the superiority of the back-illuminated CCD for low light level imaging of high resolution targets at a range of 400 meters.

## 8.0 CONCLUSION

Using CCD Transfer Curves to absolutely characterize and calibrate all of the CCD performance parameters necessary for high performance night vision applications, two high frame rate, low noise, back-illuminated CCDs manufactured using PixelVision, Inc.'s Sandbox$^{TM}$ CCD foundry service were described. The 2048 x 1024 element, split frame transfer PlutoIII CCD design and characterization was used to demonstrate the ability of large area back-illuminated CCDs to operate at video rates with high dynamic range and with low noise. Both 9-micron square pixel and 12-micron square pixel versions of the Pluto CCD were tested. A split frame transfer design with four output amplifiers was chosen as a baseline. All of the CCD parameters tested exhibited low light level imaging superior to conventional night vision technologies. Excellent cosmetic quality,

dynamic range exceeding 14 bits, linearity better than one percent, negligible dark current at video rates, nearly ideal charge transfer efficiency, and low readout noise were achieved.

Due to manufacturing tolerances, the 4.5 electrons rms. noise floor of the Pluto CCD represents a practical lower limit for large area devices. To further improve the sensitivity of back-illuminated CCDs for low light level imaging, architectures with greater than four amplifiers will be required to reduce the bandwidth of each analog channel. To demonstrate the performance and manufacturability of multiple output CCDs, the forty output amplifier ADAPTIII CCD was tested. On a majority of the devices manufactured, all of the forty amplifiers were shown to have a noise floor of approximately 4 electrons rms. or better.

Having successfully optimized the designs and processes of high resolution, large area CCDs and multiple amplifier designs, the next generation of Sandbox™ will build upon the successes of their predecessors. The Kino, 2048 x 1024, 8-output amplifier CCD has been manufactured on PixelVision, Inc.'s SandboxIV foundry run. The device is currently being tested. Low light level CCD designs with larger formats and with 32 and 64 output amplifiers will follow.

## 9.0 ACKNOWLEDGEMENTS

Jim Janesick of PixelVision Inc.'s Advanced Sensors Division, in collaboration with Taner Dosluoglu and the Advanced Development Group at Scientific Imaging Technologies, Inc., designed the Pluto and Adapt series of CCDs. Mr. Janesick was also responsible for the development of the CCD Transfer Method, as well as the test and characterization of the SandboxIII Pluto CCDs. Tom Elliott of the California Institute of Technology's Jet Propulsion Laboratory contributed a majority of the Pluto 9-micron CCD Transfer Curve test results. His work is noted where applicable. The testing and optimization of the ADAPTIII CCD were performed by Alice Reinheimer of PixelVision, Inc.'s Commercial Systems Division. The low light level comparisons and images of image intensified and back-illuminated CCD sensors reported in Section 7.0 were performed by John L. Miller and Jim Byars of FLIR Systems, Inc., and Lt. Robert Ireland of the USAF Phillips Laboratories, Kirtland AFB, NM. The authors would like to thank the directors of PixelVision, Inc. and Scientific Imaging Technologies, Inc. for their continued internal funding of advanced imaging technologies. This document was edited by Stacey Easterbrooks, PixelVision, Inc.